

RELATIONSHIP BETWEEN THE IONIZATION ENERGY AND THE RADIAL VELOCITY OF THE IONIZED GAS IN GASEOUS NEBULAE

H. E. Caicedo-Ortiz¹, H. O. Castañeda Fernandez²

We study the relationship between the radial velocity of different ionic emission lines as a function of their ionization potential for the two largest giant extragalactic HII regions in NGC 6822. Our aim is to study the spatial velocity stratification along the line of vision within the nebula.

Keywords: *ionization potential: radial velocity: HII region*

1. Introduction

The ionization structure of HII regions is determined by the ultraviolet radiation flux of O and B stars, with the atoms at the greatest degree of ionization potential being in a volume close to the source of ionization. A study of the radial velocity of emission lines based on ions with different ionization potentials can provide important insights into the velocity stratification in a given line of sight inside the nebula. Different authors [1-3] found a relation between the ionization potential of ions producing the observed emission lines and their radial velocity, in the sense that the ions with higher ionization potential present more negative radial velocities. A comparison with the kinematical properties of nearby molecular clouds and the neutral hydrogen gas can give us as insight into the process of star formation. Our aim is perform a similar study in extragalactic HII regions.

¹ Corporación Universitaria Autónoma del Cauca, Popayán, Colombia, Departamento de Ciencias Básicas, Facultad de Ingeniería, Universidad Anahuac Norte, Estado de México, México e-mail: hernando.caicedo@uniautonomia.edu.co

² Escuela Superior de Física y Matemáticas, Instituto Politécnico Nacional, México

In this article we study the kinetics of the ionized gas in two brightest giant HII regions of the galaxy NGC 6822, Hubble V and Hubble X. Hubble V and Hubble X are part of the vast complex of HII regions that are located in the north of the galaxy NGC 6822 [4,5]. With an optical size of 112 and 143pc respectively [6,7] and separation of 320pc, the objects are the two most luminous HII regions of the galaxy. The luminosity of the HII regions in $H\alpha$ is useful to estimate the star formation rate, as the regions are optically thick [8]. Studies on determination of the abundance for these regions were published in [9-12]. Castaneda and collaborators [13,14] measured the local density of the ionized gas for Hubble V and Hubble X. Caicedo and collaborators [15,16] measured the fractal dimensions in Hubble X and Hubble V. Peimbert and collaborators [17] obtained the temperature [18], density, and abundance for Hubble V and Hubble X, while the electron density has been computed from the integrated spectra of these regions [17,19]. The integrated spectrum of the whole region is used to determine the global radial velocity of the region. Our intention is to correlate the ionization potential bound with the spatial distribution of the ionized gas with the velocity of the gas.

2. Observations and Data Reduction

The raw data used in this study was obtained from the Data Center archive of the Cambridge Astronomical Survey Unit (CASU) at the Institute of Astronomy of the University of Cambridge. The long-slit spectroscopy observations were done between August 18 and 20, 1992, with the spectrograph ISIS from the William Herchel Telescope at the Roque de los Muchachos Observatory in the Canary Islands, Spain.

The spectra for different HII regions were taken with different locations of the slit, with eight positions for Hubble X, and four positions for Hubble V, all of them at a position angle of 90 degrees, with slit effective width for each of 1" and a separation from 2 to 3 arcseconds between the centers of each two consecutive positions of the slit. Two spectra were simultaneously taken for each position, one in the range between 6390Å and 6849Å (red arm) and another between 4665Å and 5065Å (blue arm), both with an approximate dispersion of 0.4Å/pixel. The exposure time for each spectrum obtained at each slit position was 1000 s for Hubble V and 1200 s for Hubble X. The slit has a length of 200" with a spatial sampling along the slit of 0.34"/pixel on the red arm (Chip EEV3) and 0.36"/pixel on the blue arm (Chip TEK1).

The data was reduced using the standard techniques (bias subtraction, flat field correction) and calibrated in wavelength, using the IRAF software¹.

Individual spectra were created by adding four consecutive one-dimensional spectra that correspond to the spatial resolution given by the seeing. Line emission profiles were analyzed using the DIPSO² package within the STARLINK software. A single Gaussian fitting was performed over each spectrum.

¹ IRAF is distributed by the National Optical Astronomy Observatories, which are operated by the Association of Universities for Research in Astronomy, Inc., under contract to the National Science Foundation.

² Available in <http://star-www.rl.ac.uk/>.

3. Emission Flux Maps

From the spectra obtained for each position in the nebulae we produced the two-dimensional intensity maps for different emission lines observed with use of the interpolation method proposed in [20]. The emission maps in Figs. 1-4 show the maps for the central area of the region for the emission lines $H\alpha$ created from the observations used in this work. The maps show excellent agreement with the images in $H\alpha$ for Hubble V and Hubble X in [21].

The long-slit spectra were added to create a single global spectrum for the central region of each object. The integrated spectra for Hubble V and Hubble X are shown in Figs. 5 and 6. Again the analysis of the line was performed with DIPSO, fitting a single Gaussian and a lineal continuun. In the case of line doublets we only proceeded to fit the more intense line.

From the Gaussian fit in different lines of emission, the Doppler radial velocities are determined for the different emission lines observed in Hubble V and Hubble X. The data were corrected to the value of heliocentric velocity ($v_{helio} = v$). We estimate that the radial velocity error is of the order of 2 km/s ($0.04\text{\AA}/\text{pixel}$). Table 1 shows the different radial velocities of each of the ions studied in Hubble V and Hubble X.

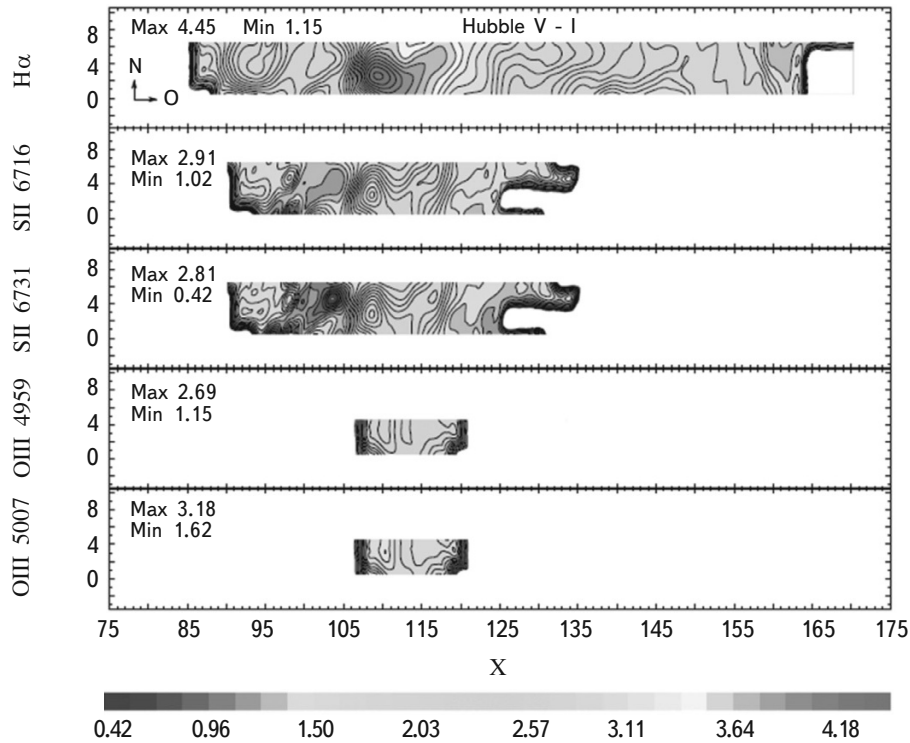


Fig.1. Maps of the emission for the central zone of Hubble V in $H\alpha$, [SII] $\lambda\lambda$ 6717, 6731, and [OIII] $\lambda\lambda$ 4959, 5007. The contour scale is logarithmic.

TABLE 1. Radial Velocity of Hubble V and Hubble X With Integrated Spectra

Line of emission	Hubble V (km/s)	Hubble X (km/s)	Ionization potential (eV)
H α	-56 ± 2	-49 ± 2	13.6
[SII] λ 6717	-57 ± 2	-47 ± 2	23.3
[HeI] λ 6678	-51 ± 3	-49 ± 3	24.7
[NII] λ 6548	-62 ± 2	-53 ± 2	29.6
[OIII] λ 5007	-55 ± 2	-53 ± 1	35.1

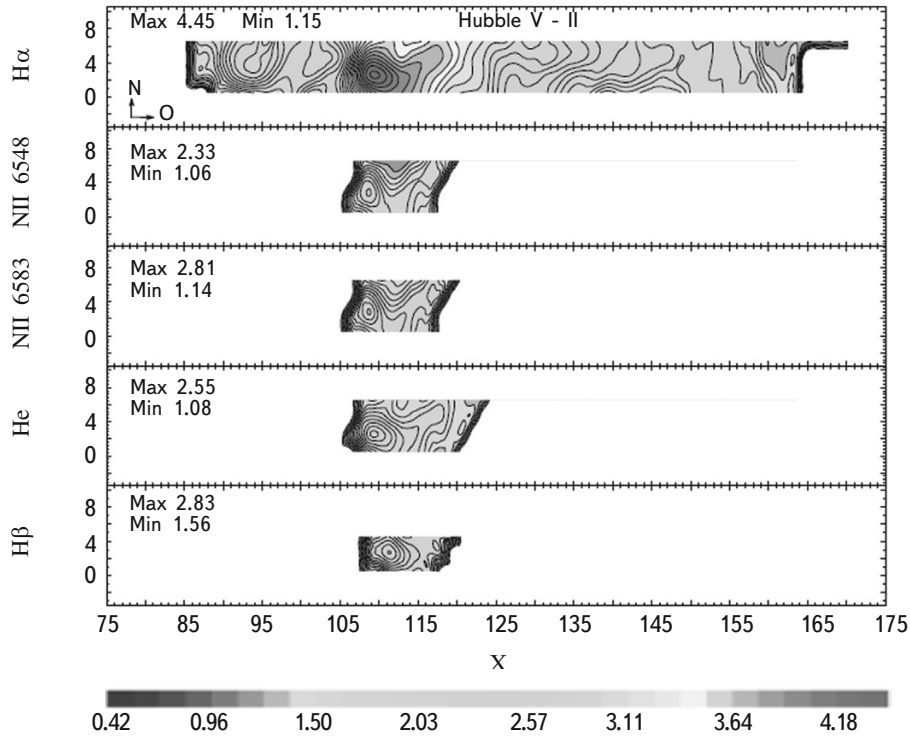


Fig.2. Maps of the emission for the central zone of Hubble V in H α , [NII] $\lambda\lambda$ 6548, 6583, He, and H β . The contour scale is logarithmic.

4. The radial velocity vs. the ionization potential

The radial velocities vs. the ionization energy (see Table 2 of [3]) of different ionization states of the elements studied in Hubble V and Hubble X are shown in Figs. 7 and 8. There is a relationship between the ionization potential and the radial velocity for the different emission lines of the ionic species. Ions with the highest potential of ionization

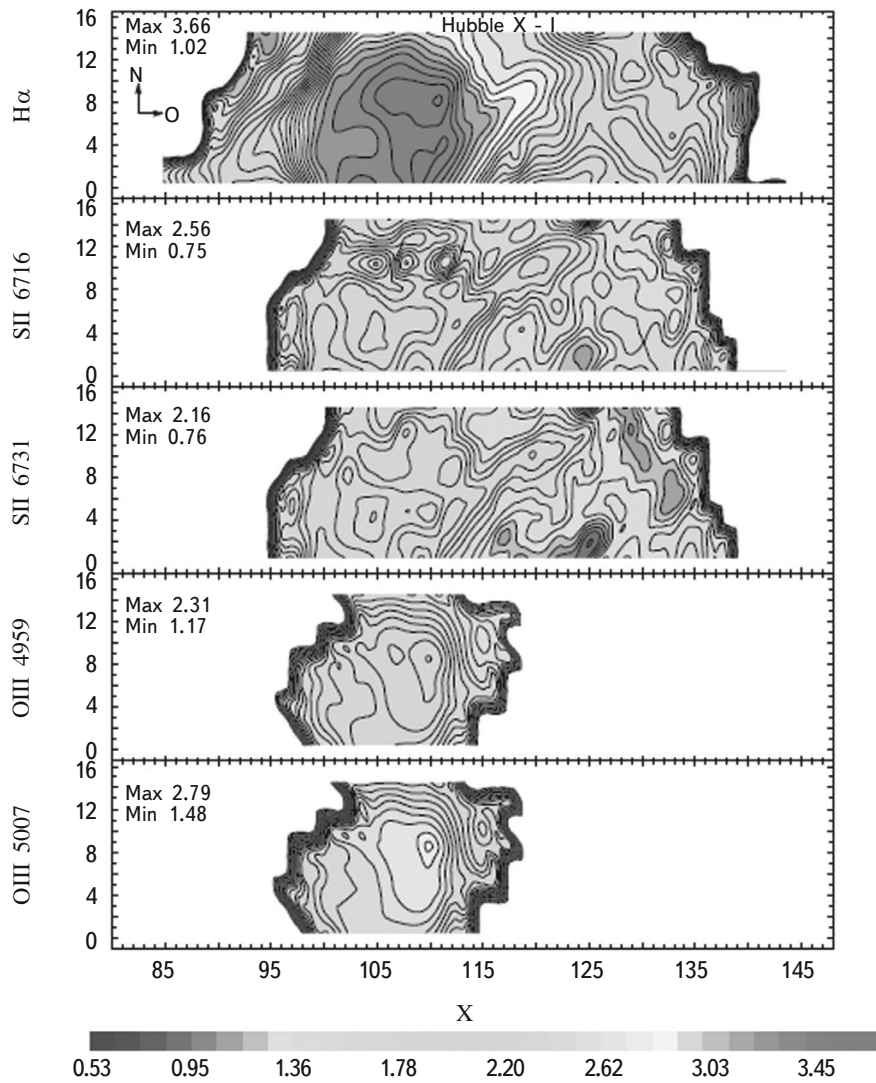


Fig.3. Maps of the emission for the central zone of Hubble X in H α , [SII] $\lambda\lambda$ 6717, 6731, and [OIII] $\lambda\lambda$ 4959, 5007. The contour scale is logarithmic.

exhibit more negative radial velocities, indicating the existence of a stratification of the radial velocity of the various gases along the line of sight. A similar behavior has been observed in galactic HII regions ([1,3] and cited references).

The likely scenario that explains this kinematical behavior of the material is the flow of ionized gas from the molecular cloud in the direction of the observer. In this model [2,22,23] the neutral species and the low ionization gas near the ionization front are at rest or moving with the molecular cloud, while the high excitation material that is near to the ionizing stars moves away from the neutral gas with velocities near the order of the speed of sound. The model explains the negative systematic difference of the radial velocity between the species of high and low ionization. This difference could simply be due to the fact that it is only possible to see the HII regions that are in

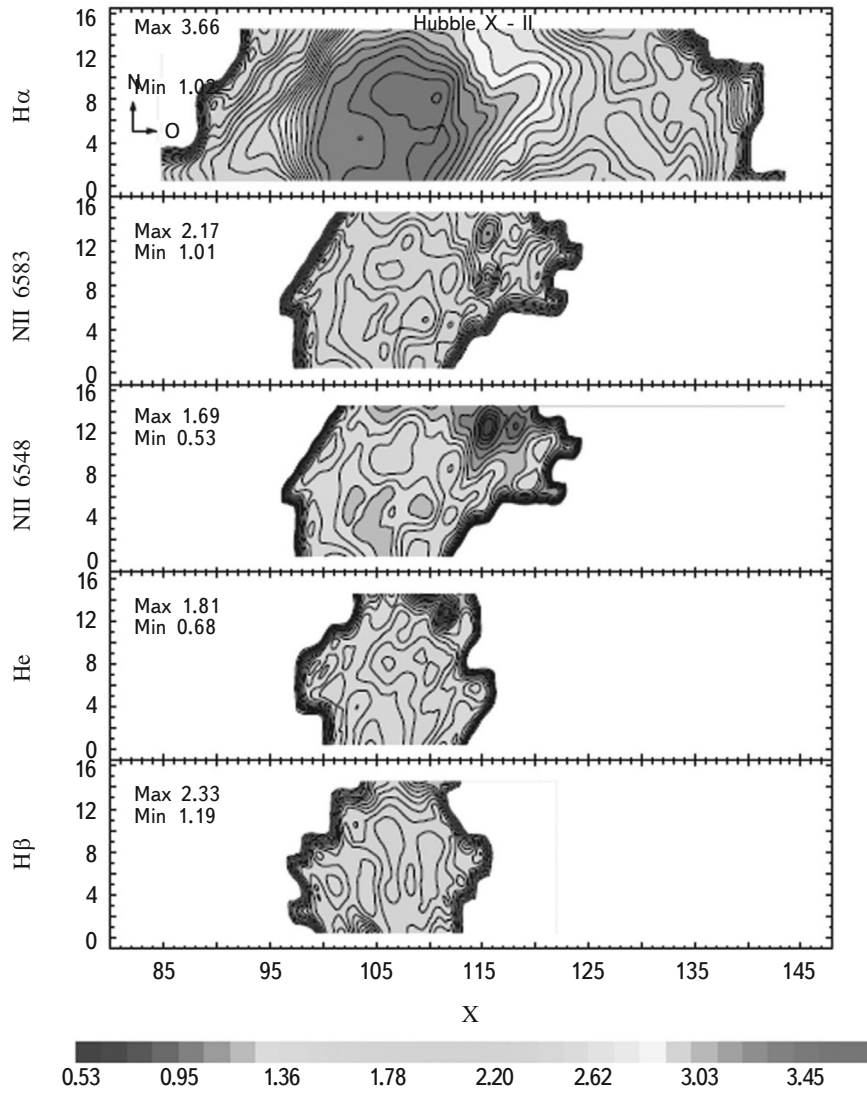


Fig.4. Maps of the emission for the central zone of Hubble V in $H\alpha$, $[NII] \lambda\lambda 6548, 6583$, He, and $H\beta$. The contour scale is logarithmic.

front of the molecular clouds. In this case, the nebulae must be limited in density in our direction, which implies that a significant fraction of the ionizing photons of these HII regions are lost in the diffuse interstellar medium, which is in agreement with evidence from the $H\alpha$ flux of the diffused ionized regions of the galaxy, where it is estimated that about 80% of the ionizing photons are lost by HII regions and emitted towards the low-density interstellar medium [24].

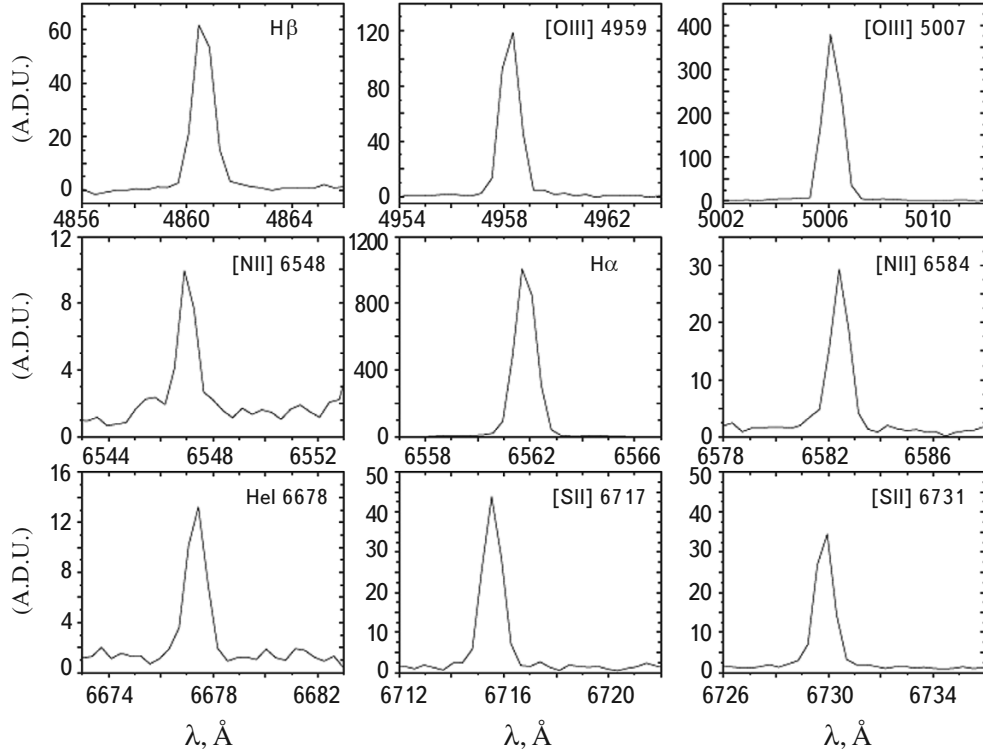


Fig.5. The integrated spectra for Hubble V.

5. Discussion

For H_2 Lee et al. [25] conducted a study in the near-infrared Hubble V, which indicates the structure of the photodissociation region (PDR), characterized by compact emission of He ($2.0587\mu\text{m}$) and $\text{Br}\gamma$ ($2.1661\mu\text{m}$), surrounded by a layer of molecular hydrogen (H_2). Table 1 of [25] presented the speed v_{LSR} , σ and the intensity of the lines $H_2 1 - 0S(1)$ and $H_2 2 - 1S(1)$ observed in five different positions of the slit oriented in the direction North-South over Hubble V (see Fig.1f of [25]). The average v_{hel} is -49 km/s.

The detection of a compact molecular cloud associated with Hubble V was first noted by [26]. Later work has reported observations of various emission lines for Hubble V at $^{12}\text{CO}(1 \rightarrow 0)$ by Israel [27], $^{12}\text{CO}(2 \rightarrow 1)$, $^{12}\text{CO}(4 \rightarrow 3)$ and $^{13}\text{CO}(1 \rightarrow 0)$, $^{12}\text{CO}(3 \rightarrow 2)$ by [28,29] and $^{12}\text{CO}(1 \rightarrow 0)$, and $^{12}\text{CO}(2 \rightarrow 1)$ by [28]. Due to the low luminosity of Hubble X, few measurements were obtained for this HII region.

One of the properties of the maps of emission of ^{12}CO presented by [29] and the map published by [26] is that they are consistent with the emission of H_2 described in Fig.1f of [25] and the extension of the emission of CO is limited but comparable to the extension of the ionized gas of Hubble V [28]. In Fig.4 of [28] the velocity maps in Hubble V for $\text{CO } J = 2 - 1$, $\text{CO } J = 3 - 2$, and $\text{CO } J = 4 - 2$ are in a range of v_{hel} between -43 km/s and -63 km/s. The velocities observed for different CO lines are in the same range as the velocities of ionic species

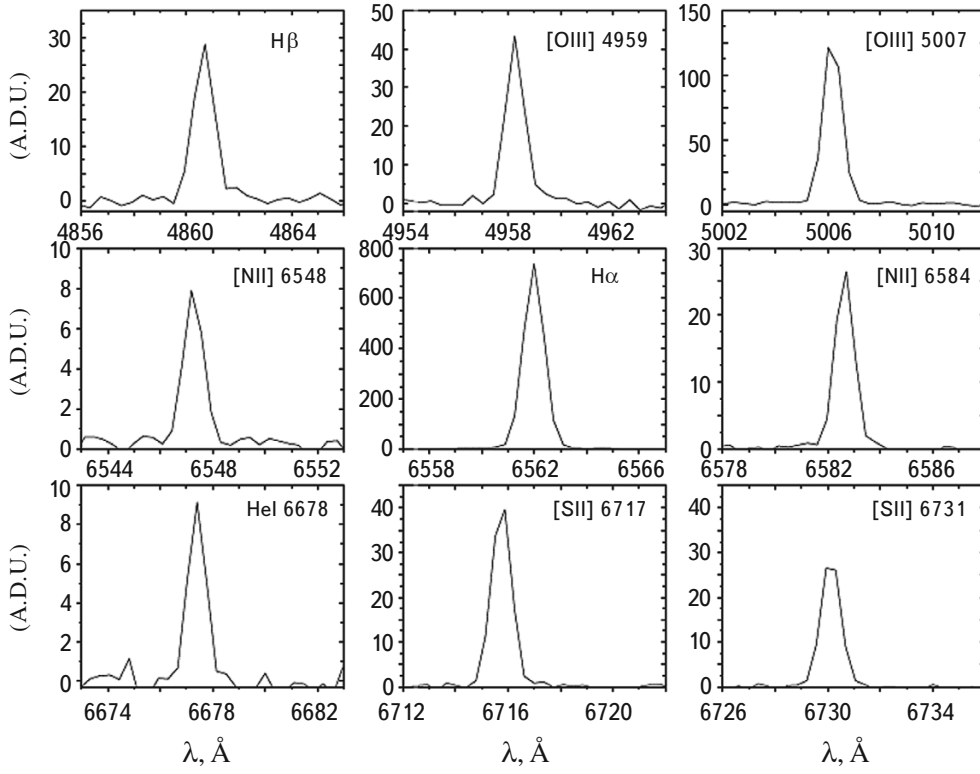


Fig.6. The integrated spectra for Hubble X.

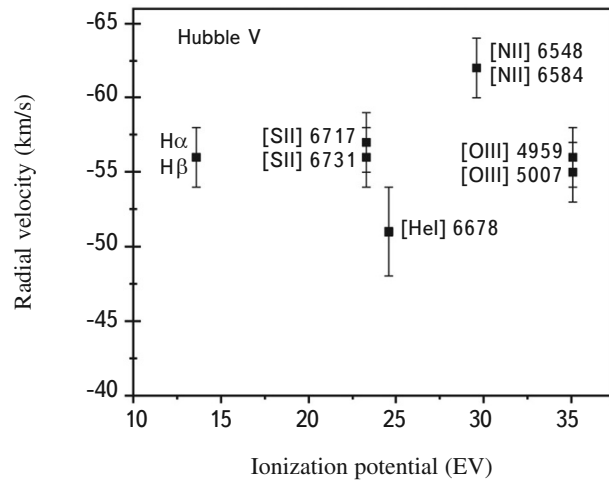


Fig.7. Radial velocity vs ionization potential for the different emission lines in Hubble V.

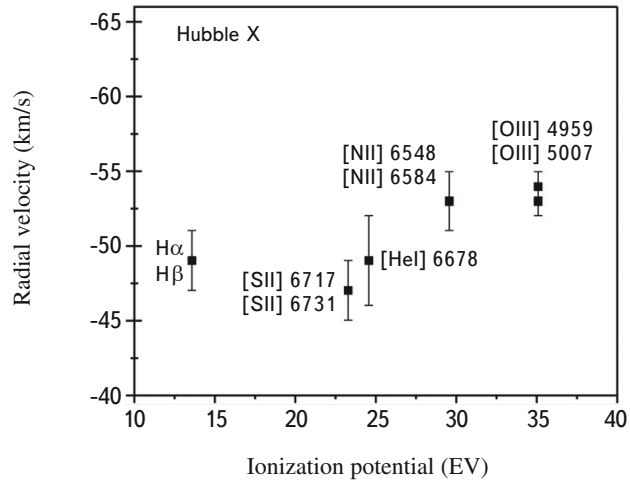


Fig.8. Radial velocity vs ionization potential for the different emission lines for Hubble X.

observed in this study, as well as those seen in H₂ by Lee [25]. This last relationship between the cold molecular gas (traced by CO) and H₂ implies that there is no detectable activity of young stellar objects around the core of Hubble V [25].

We have identified the HII regions Hubble V and Hubble X. The velocity of the HI gas that is associated to the HII regions was computed by interpolation of the data available. The heliocentric velocity range in our data for

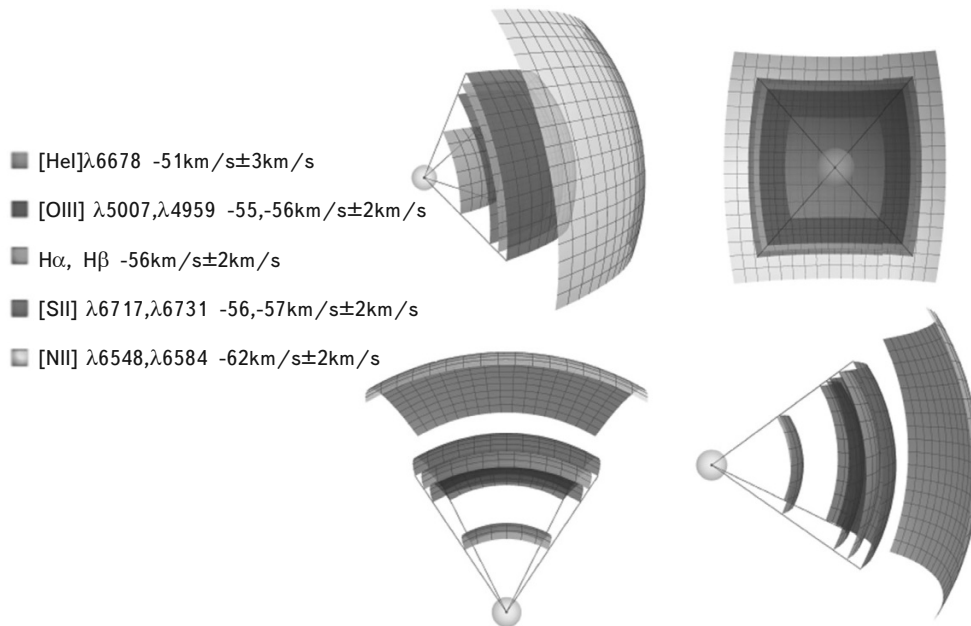


Fig.9. 3D model of the radial velocity stratification for Hubble V.

Hubble V is located between -55 km/s and -65 km/s, while for Hubble X its velocity range is between -45 km/s and -55 km/s. These velocity ranges are consistent with the range resolution of the observations made by Gottesman, which is $2'.3$ (330 pc) [30]. From the data in Fig.4 of [30], we compute the average value of the radial velocity of HI of -60 km/s for Hubble V, and -51 km/s for Hubble X.

Saito [31] suggested that the movement of the HII regions in relation to the surrounding HI gas may provide clues for understanding the mechanisms associated with the star formation in galaxies of this type. For the IC 10 galaxy it was found that the velocity of the HII gas is of the order of 5 km/s larger than the surrounding gas, and similar to the associated CO molecular clouds [31]. From Table 1 we note that the radial velocity of HI is larger than the integrated velocity of $H\alpha$ in Hubble V and Hubble X, indicating a relative movement of the HII regions with respect to the HI gas [7]. The radial velocity of the CO is of the same order as $H\alpha$.

With all these elements, it is possible to create a simple model based on the observed radial velocities of the different ionic species detected in Hubble V and Hubble X.

The Hubble V structure, seen in the direction of the observer towards the molecular cloud, has a first layer of [NII] moving at (-62 ± 2) km/s. The second layer consists of [OIII], [SII], and HII, moving at a speed of (-56 ± 2) km/s and finally a third layer of HeI moving at a velocity of (-51 ± 2) km/s. Figure 9 presents a three-dimensional model of the velocity stratification for Hubble V.

For Hubble X, as in Hubble V, the first layer is made up of [NII] and [OIII] moving at a speed of (-53 ± 2) km/s. The second layer consists of HII, with a speed of (-49 ± 2) km/s. The third layer is HeI moving to (-49 ± 3) km/s, and finally a fourth layer of [SII] that moves at a speed of (-47 ± 2) km/s. Figure 10 presents a three-dimensional model of the velocity stratification for Hubble X.

6. Conclusions

A relationship has been obtained between the heliocentric radial velocity and the ionization potential for different ionic species. This result indicates a stratification in radial velocities along the line of sight.

A study with a larger number of HII regions in which it is possible to observe several emission lines such as those reported by Esteban [32] allows to find a mathematical model that describes the functional relationship between these two parameters, which in the present work is not possible to carry out by the small number of HII regions and regions studied. However, it is clear that such a relationship exists.

The $H\alpha$ radial velocity is of the same order as the velocity of the CO clouds associated to the nebulae. A comparison of $H\alpha$, CO, and HI indicates that the cloud is infalling toward the HI gas.

Acknowledgments

This work was supported in part by the Secretaria de Investigacion y Posgrado del IPN, under the projects SIP-20161743 y SIP-20171070.

REFERENCES

1. J. B. Kaler, *Astrophys. J.*, **148**, 925, 1967.
2. C. R. O'Dell and Z. Wen, *Astrophys. J.*, **387**, 229, 1992.
3. C. Esteban and M. Peimbert, *Astron. Astrophys.*, **349**, 276, 1999.
4. E. P. Hubble, *Astrophys. J.*, **62**, 409, 1925.
5. P. Hodge, M. G. Lee, and R. C. Kennicutt, *Publ. Astron. Soc. Pacif.*, **100**, 917, 1988.
6. P. Hodge, M. G. Lee, and R. C. Kennicutt, *Publ. Astron. Soc. Pacif.*, **101**, 32, 1989.
7. A. Tomita and K. Ohta, M.Saito, *PASJ*, **45**, 693, 1993.
8. C. R. O'Dell, P. W. Hodge, and R. C. Kennicutt, *Publ. Astron. Soc. Pacif.*, **111**, 1382, 1999.
9. B. E. J. Pagel, M. G. Edmunds, and G. Smith, *Mon. Not. Roy. Astron. Soc.*, **193**, 219, 1980.
10. M. Peimbert and H. Spinrad, *Astron. Astrophys.*, **7**, 311, 1970.
11. H. E. Smith, *Astrophys. J.*, **199**, 591, 1975.
12. J. Lequeux, M. Peimbert, J. F. Rayo et al., *Astron. Astrophys.*, **80**, 155, 1979.
13. H. O. Castañeda, H. E. Caicedo-Ortiz, and J. P. Oregón, In *Rev. Mex. Astron. y Astrofíz. Conf. Ser.*, **44**, 16, 2014.
14. J. P. Oregón, H. E. Caicedo-Ortiz, H. O. Castañeda, and A. M. Hidalgo-Gómez, *J. Cien. Ing.*, **6**(1), 16, 2014.
15. H. E. Caicedo-Ortiz, E. Santiago-Cortés, J. López-Bonilla, and H. O. Castañeda, *Journ. Phys.: Conf. Ser.*, **582**, 012049. IOP Publishing, 2015.
16. H. E. Caicedo-Ortiz, H. O. Castañeda, and E. Santiago-Cortés, *Rev. Bras. Ens. Fís.*, **39**(3), 2017.
17. A. Peimbert, M. Peimbert, and M. T. Ruiz, *Astrophys. J.*, **634**, 1056, 2005.
18. A. M. Hidalgo-Gómez, K. Olofsson, and J. Masegosa, *Astron. Astrophys.*, **367**, 388, 2001.
19. H. O. Castañeda, J. M. Vilchez, and M. V. F. Copetti, *Astron. Astrophys.*, **260**, 370, 1992.
20. A. K. Cline and R. L. Renka, *J. Math.*, **14**, 119, 1984.
21. J. Collier and P. Hodge, *Astrophys. J. Suppl. Ser.*, **92**, 119, 1994.
22. B. Zuckerman, *Astrophys. J.*, **183**, 863, 1973.
23. B. Balick, R. H. Gammon, and R. M. Hjellming, *Publ. Astron. Soc. Pacif.*, **86**, 616, 1974.
24. C. G. Hoopes, and R. A. M. Waltherbos, *Astrophys. J.*, **586**, 902, 2003.
25. S. Lee, S. Pak, S.-G. Lee et al., *Mon. Not. Roy. Astron. Soc.*, **361**, 1273, 2005.
26. C. D. Wilson, *Astrophys. J.*, **434**, L11, 1994.
27. F. P. Israel, *Astron. Astrophys.*, **317**, 65, 1997.
28. F. P. Israel, F. Baas, R. J. Rudy et al., *Astron. Astrophys.*, **397**, 87, 2003.

29. S. de Rijcke, P. Buyle, J. Cannon et al., *Astron. Astrophys.*, **454**, L111, 2006.
30. S. T. Gottesman and L. Weliachew, *Astron. Astrophys.*, **61**, 523, 1977.
31. M. Saito, M. Sasaki, K. Ohta et al., *PASJ*, **44**, 593, 1992.
32. C. Esteban, F. Bresolin, and M. Peimbert, *Astrophys. J.*, **700**, 654, 2009.